This article has been accepted for inclusion in a future issue of this journal. Content is final as presented, with the exception of pagination.

Elastic Force Compensation via Negative Stiffness Mechanism for the ECRH Steering Launcher of DTT

Daniele Busi, Stefano Cogliati, Francesco Braghin, *Member, IEEE*, Alessandro Bruschi, Francesco Fanale, Gustavo Granucci, Afra Romano, and Fabio Zanon

***Abstract*—The full power configuration of the Divertor Tokamak Test (DTT) facility will include 32 independent electron cyclotron resonance heating (ECRH) front-steering launching mirrors. A highly compact, 2-degree-of-freedom steering mechanism based on in-vessel piezoelectric walking drives is currently under design. This solution is intended to minimize space occupation within the ports—allowing for the launchers to fit within the limited DTT duct space—while optimizing dynamic performance and control bandwidth. Wherever feasible, flexures replace traditional hinges, with the combined advantages of eliminating wear and backlash, thus extending component lifespan and enhancing steering accuracy. At the same time, flexible joints introduce elastic resistance to the steering motion, which must be counteracted by the actuators. This reduces the force available for resisting other external disturbances, like electromagnetic (EM) loads. In order to mitigate elastic resistance, a negative-stiffness element called oblique-spring stiffness compensator (OSSC) is proposed. The static analysis of the device is presented, optimal design rules are identified, and the conceptual design of a prototype integrated in the launcher assembly is shown. The target of the study is the realization of a statically balanced steering mechanism that retains the main benefits of compliant joints, namely the absence of wear, backlash, and joint friction, without incurring the usual penalty of elastic resistance and loss of available driving force.**

***Index Terms*—Divertor tokamak test (DTT), electron cyclotron resonance heating (ECRH) launcher, fusion, negative stiffness, static balancing, stiffness compensator.**

I. Introduction

THE Divertor Tokamak Test facility (DTT) [1] will incorporate a powerful Electron Cyclotron Resonance Heating (ECRH) system, capable of coupling 28.8 MW to the plasma at full power, via 32 microwave beam lines (1 MW, 170 GHz) with 90% transmission efficiency [2]. During the 100 s DTT pulses (50 s flat-top), the system will serve various tasks, among which are bulk heating and current drive, plasma current start-up, and magneto-hydrodynamic (MHD) control. Each line ends with an actively cooled front-steering launcher, which includes a fixed focusing mirror M1 and a double-steering flat mirror M2. All 32 launchers are configured as identical modules to simplify design and integration while reducing procurement costs [3].

Received 30 September 2025; revised 1 May 2026; accepted 22 June 2026. The review of this article was arranged by Senior Editor M. Kovari. *(Corresponding author: Daniele Busi.)*

Daniele Busi, Stefano Cogliati, and Francesco Braghin are with the Department of Mechanical Engineering, Politecnico di Milano, 20156 Milan, Italy (e-mail: daniele.busi@polimi.it).

Alessandro Bruschi and Francesco Fanale are with the Institute of Plasma Science and Technology–CNR, 20125 Milan, Italy.

Gustavo Granucci is with the Institute of Plasma Science and Technology–CNR, 20125 Milan, Italy, and also with DTT S.C. a r.l., 00044 Frascati, Italy.

Afra Romano is with the Fusion and Nuclear Safety Department, ENEA, 00044 Frascati, Italy, and also with DTT S.C. a r.l., 00044 Frascati, Italy.

Fabio Zanon is with Eni S.p.A., 30175 Venice, Italy.

Color versions of one or more figures in this article are available at https://doi.org/10.1109/TPS.2026.3707200.

Digital Object Identifier 10.1109/TPS.2026.3707200

A. Launcher Requirements and Working Environment

M2 poloidal and toroidal mechanical (optical) ranges are 17.5° (35°) and 50° (50°), respectively, ensuring that all modules can potentially carry out all the above-mentioned tasks independently, for enhanced experimental flexibility. The maximum poloidal and toroidal mechanical (optical) steering speeds are 20°/s (40°/s) and 12°/s (12°/s), respectively, as justified by task-switching and MHD control needs [2]. The required mechanical steering resolution is 0.05° and 0.1° for poloidal and toroidal rotations, respectively. This ensures that the vertical and horizontal positioning resolution of the power deposition spot in the plasma is lower than 10 mm.

The working environment is affected by thermal, nuclear, and electromagnetic (EM) loads. The mirror is subjected to a Gaussian heat flux on its reflective surface due to microwave absorption, which adds to plasma radiation for a total of $\approx 15\,\mathrm{kW}$ with a $2\,\mathrm{MW/m^2}$ peak in the center. Stray radiation heat flux from microwaves and plasma is estimated around $15\,\mathrm{kW/m^2}$ for all components in the ports [4]. Nuclear heating is negligible ($< 0.01\,\mathrm{W/cm^3}$) and ($> 0.1\,\mathrm{MeV}$) neutron fluence is $1.13 \cdot 10^{17}\,\mathrm{cm^{-2}}$ at DTT end-of-life, corresponding to $2 \cdot 10^{-4}$ dpa [5].

The static magnetic field during plasma flat top at M2 is 4 T, decreasing down to 150 mT at the cryostat on the equatorial plane. The most critical EM loads are related to Major Disruption events with 6 ms current quench. In this scenario, vertical field variations of 200 T/s are expected at M2 location.

B. Piezo-Based Launcher Description

Due to the large number of launcher modules relative to the size of the machine, the design of the steering mechanism must resort to a compact solution. One of the options under study is based on in-vessel piezoelectric walking drives [6], as

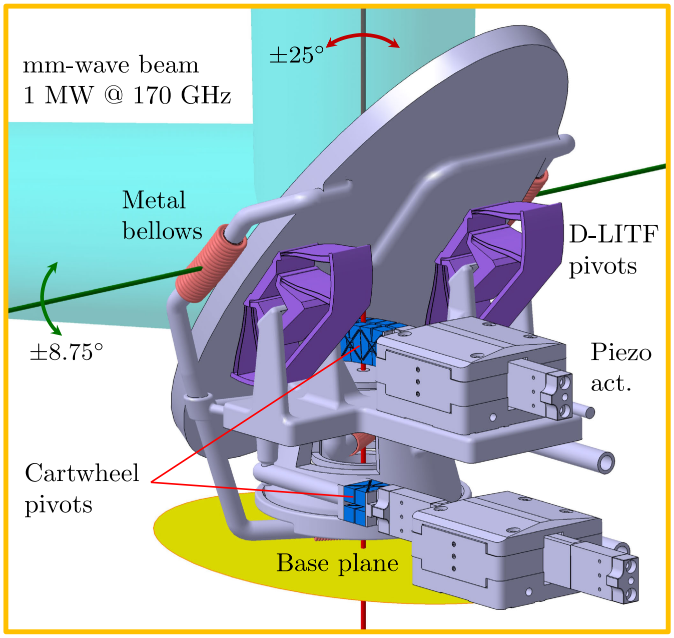

Fig. 1. CAD model of the piezo-based steering mechanism with the M2 mirror.

represented in Fig. 1. This allows limiting the total mass of a launcher module to less than 5 kg, by avoiding the long transmission shafts traditionally used to connect external motors to the mirror [7], [8], [9]. Walking drives are mechatronic devices in which piezoelectric "legs" are deformed in a coordinated way via electric fields to press against a slider and move it step by step along a linear trajectory. In the case of the UHV-compatible PI N-331 drive [10] selected for this application, each step is up to 25 μm long and the stepping frequency is up to 600 Hz, for a maximum slider speed of 15 mm/s. The "feet" at the base of the "legs" are preloaded against the slider, so that its position is fixed by static friction even when the actuator is powered off. On the other hand, reliance on static friction imposes an upper limit (adherence) to the force that can be transmitted in the direction of motion. If the adherence limit is overcome by external forces (including inertia), the slider slips under the "feet" and position control is lost. This situation must be avoided by design, ensuring that external forces during operation are reduced well below the adherence limit, which, in case of the PI N-331 actuator, is 50 N. We will refer to this quantity as the *force budget*. An exception to this rule can be allowed in case of disruption events, during which position control is not necessary, leaving the integrity of the steering system as the only requirement.

C. Force Budget

The force budget must be shared among all sources of mechanical loads, including inertia, EM loads, hydraulic forces, joint friction, and elastic resistance.

1) EM Loads: EM loads can be mitigated by a proper steering mirror design, given the rules outlined in [11]. The current design of M2 is based on the traditional solution of a stainless-steel substrate with Variable-Depth Complementary Spiral internal channels [12], [13] with a superficial Copper insert, as represented in Fig. 2. This solution is appealing for the relative simplicity of manufacturing and previous use in other machines [7], [8], [9], [14]. The stainless-steel substrate serves as an EM load mitigator, while the Copper insert reduces thermal stresses by uniformly distributing the heat load on the substrate. A micrometric Copper or Gold coating on mirror surface ensures efficient microwave reflection. During operation, EM loads are mainly caused by magnetic braking, external radial fields with sinusoidal time-variation induced by nonaxisymmetric coils, and plasma current variations associated with MHD equilibrium evolution and high-to-low confinement mode transitions. When considering the superposition of all these factors, EM calculations [11] give worst case 30.6 and 38.2 N forces acting on the poloidal and toroidal actuators, respectively.

2) Hydraulic Loads: Due to compactness requirements, the cooling system makes use of multilayer corrugated metal bellows to feed water to the steering mirror. In order to decrease the risk of water leakages, the option of double-bellows with monitored interspace, as advised by the ITER Vacuum Handbook [15], is being studied. The bellows are positioned in such a way that their geometric center is aligned with the axis of rotation of the mirror, in order to undergo almost pure bending deformation during mirror rotations. This has the additional benefit of producing no hydraulic torque on the mirror, as both the longitudinal and transverse hydraulic forces that develop in the bellows act on mirror rotation axes. Therefore, this configuration virtually implies complete absorption of hydraulic loads by mirror supports, with no effects on the actuators. Future studies will quantify the manufacturing and assembly tolerances needed to reduce parasitic hydraulic loads to negligible levels.

3) Elastic Loads: In order to avoid detrimental effects related to friction and backlash, like wear and loss of positioning precision over time, a monolithic, fully compliant version of the poloidal mechanism is under design, while the wide toroidal rotations are accommodated by ceramic bearings. Compliant mechanisms introduce challenges related to fatigue failure risk and elastic resistance, the latter of which is of interest for this work. The flexures resist deformation and produce an elastic force F_e on the poloidal actuator in the form

$$F_e(x) = -k(x)\,x \tag{1}$$

where x is the (forward) direction of motion of the poloidal slider and $k(x)$ is a position-dependent equivalent stiffness term that can be derived analytically from the kinematic arrangement of the mechanism. The main contribution to k comes from the Double-Leaf Type Isosceles Trapezoidal Flexure (D-LITF) pivots [16] employed as Remote Center of Motion mirror supports (purple in Fig. 1), which are expected to provide about 15 N of elastic resistance to the poloidal actuator at maximum poloidal rotation. An additional force of about 2 N is provided by bellows and *cartwheel* pivots (pink and blue in Fig. 1, respectively), which are used as pins in the poloidal crank-shaft transmission [6]. Therefore, a total elastic force of 17 N is expected on the poloidal actuator at its maximum displacement, which is 6.5 mm, for a total equivalent stiffness k = 2.6 N/mm [17]. Since $k(x)$ shows

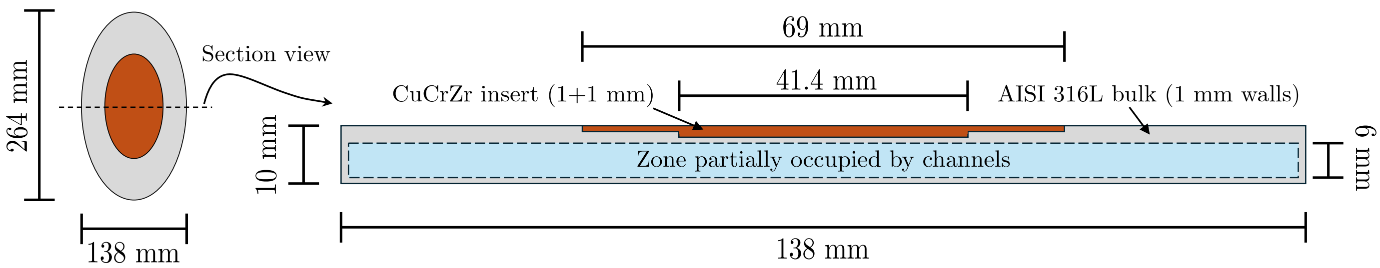

Fig. 2. Geometry of the metallic version of M2 currently under consideration.

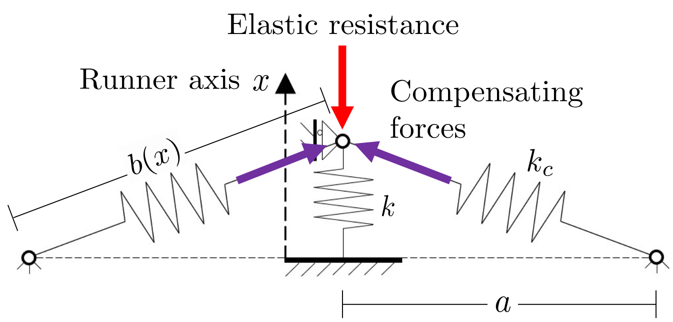

Fig. 3. Scheme of an OSSC with $n = 2$ compensation springs.

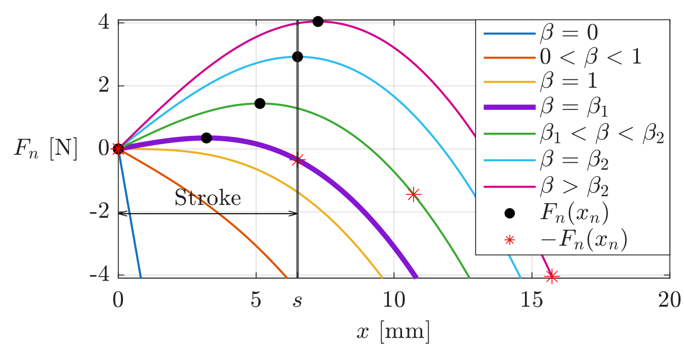

Fig. 4. $F_n(x)$ for different β values in the positive half-plane, given arbitrary values of $s = 6.5$ mm, $a = 21.67$ mm, and $k_0 = 5$ N/mm.

little variation (<6%) across x domain, it will be considered constant for the sake of simplicity in this work. Negligible elastic force is applied to the toroidal actuator.

4) Grand Total: If we superimpose the contributions of EM disturbances and elastic resistance, we get a worst case force of about 47.6 N acting on the poloidal actuator, which is dangerously close to the limit value of 50 N, with a safety factor of only 1.05. This work presents a possible solution to this problem, based on the concept of *static balancing*, or *stiffness compensation*. This method involves adding a negative-stiffness element to the mechanical transmission, tuned to offset the positive stiffness of the other deformable parts, such that the net elastic force F_n acting on the poloidal actuator is

$$F_n(x) = -\left(k(x) + k_{\text{comp}}(x)\right) x \qquad \text{with} \quad k_{\text{comp}} < 0. \tag{2}$$

If properly sized, a stiffness compensator allows reducing the external disturbances acting on the poloidal actuator to less than 35 N, increasing the safety factor to 1.47, as shown in the following.

D. Static Balancing Solutions

Passive compensation of elastic forces is largely associated with vibration isolation technology. Quasi-Zero Stiffness (QZS) mechanisms can be realized with oblique springs or rods, repelling magnets, or buckled beams [18]. It is important to notice that these devices generally have a nonlinear force-displacement characteristic, typically an odd function with one stationary point in the positive half-plane (a relevant example is shown in Fig. 4), implying that exact zero tangent stiffness is only achieved at a single displacement value, where the force-displacement curve is flat. Indeed, for any $F_n(x)$, the tangent stiffness is

$$k_t(x) = -\frac{\mathrm{d}F_n}{\mathrm{d}x} \tag{3}$$

which is null in the stationary points of $F_n(x)$. In the same way, it is only possible to obtain exact elastic force compensation at unique points, corresponding to the roots of the characteristic curve, where $F_n(x) = 0$ due to exact cancellation between k and k_{comp}.

In the field of vibration isolation, the target is to reduce the natural frequency ω_0 of a mechanism to zero in the neighborhood of a given equilibrium position x_0, which defines the range of displacements observed during vibration. If $m(x_0)$ is the equivalent mass of the mechanism at x_0, then

$$\omega_0 = \sqrt{\frac{k_t(x_0)}{m(x_0)}}. \tag{4}$$

Therefore, QZS mechanisms are tuned to work in the zero tangent stiffness regime $k_t(x_0) = 0$, i.e., the stationary point of the $F_n(x)$ curve.

In the case of the DTT ECRH launcher instead, the target is different: rather than concentrating on vibration reduction at a particular x_0 position, we are interested in minimizing elastic resistance throughout the entire stroke of the actuator, which is the full domain of x, in order to stay as far as possible from hitting the adherence limit. Therefore, we have to tune the stiffness compensator to minimize the maximum of $|F_n(x)|$, considering the full nonlinear characteristic curve to find suitable optimality conditions.

Among the possible solutions, the oblique spring configuration fits well the requirements of the launcher, as it does not contain magnetic elements, it is compact, and it only includes simple pins and compression springs. In this work, the oblique-spring stiffness compensator (OSSC) is investigated as a compact passive element for reducing the peak elastic load transmitted to the DTT launcher poloidal actuator, and simple sizing rules are derived for its preliminary design.

II. Modeling

A. Compensator Description

A scheme of the OSSC is given in Fig. 3. A slider (the poloidal actuator's runner) constrained to move in the x direction is connected to the ground (the toroidally rotating base to which the actuator is fixed) through a spring of stiffness k (the equivalent stiffness of D-LITF mirror supports, bellows and cartwheels), called the *main spring*. When $x = 0$, the main spring is at rest. A positive integer number n of identical *compensation springs* of stiffness k_c, encapsulated in sleeves with free length b_0 and deformed length $b(x)$, are pinned to the slider and to ground in transverse direction. When $x = 0$, the compensation springs are pre-compressed to a length $b(0) = a$. Since their direction when $x = 0$ is perpendicular to the x axis, no force is projected in the x direction. When the slider moves to $x > 0$, the x-projection of the preload of each compensation spring becomes positive, producing a force contribution $F_c(x)$ along the x axis that partially compensates the negative force contribution kx exerted by the main spring. The magnitude of the net elastic force $F_n(x) = F_c(x) - kx$ will be lower than the uncompensated force kx as far as there is residual preload in the compensation springs, which is true for $b(x) < b_0$. The main target of the present study is to minimize the maximum magnitude of the net elastic force within a prescribed symmetric stroke $x \in [-s, s]$.

B. Tuning the Net Force Curve

The expression of the net elastic force F_n acting on the slider toward the positive x direction can be easily computed through the principle of virtual works or by static equilibrium equations, which yield

$$F_n(x) = k_0 x \left(\frac{\beta}{\sqrt{(x/a)^2 + 1}} - 1 \right) \tag{5}$$

$$k_0 = k + nk_c \qquad \beta = \frac{b_0 n k_c}{a k_0}. \tag{6}$$

The force characteristic depends on three parameters (e.g., a, β, k_0), which are also related to other relevant quantities, like the transverse preload force P applied to each compensation spring and their precompression ΔL_c

$$P = k_c \Delta L_c = a \frac{k_0(\beta - 1) + k}{n} \tag{7}$$

$$\Delta L_c = b_0 - a = a \left(\frac{\beta k_0}{k_0 - k} - 1 \right). \tag{8}$$

$F_n(x)$ is represented in Fig. 4 for increasing values of β. It is an odd function with stationary points in $\pm x_n$. The stationary points degenerate into a single inflection point in the origin for $\beta = 1$, while for $\beta > 1$ there is a maximum (minimum) in the positive (negative) half-plane. The function is monotonically decreasing for $\beta < 1$. Since x_n increases with β, there exists one $\beta = \beta_2$ for which $x_n = s$. Moreover, since $F_n(x)$ decreases for $x > x_n$, we must also deduce that there must be a value $\beta = \beta_1 < \beta_2$ for which

$$F_n(s) = -F_n(x_n) \iff \beta = \beta_1. \tag{9}$$

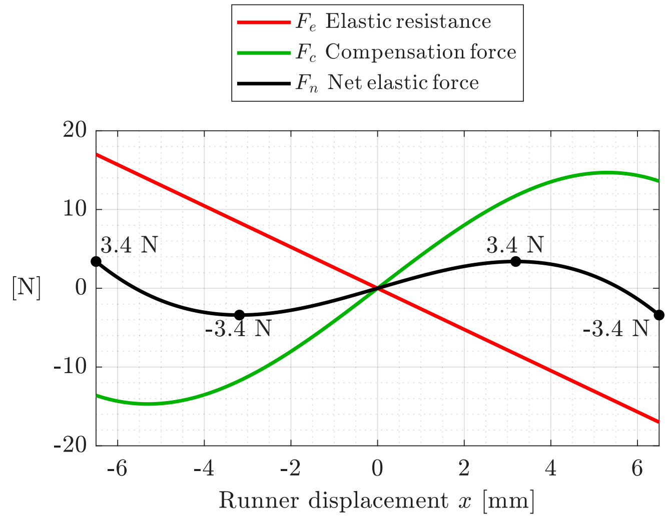

Fig. 5. Trend of elastic forces resulting from prototype design.

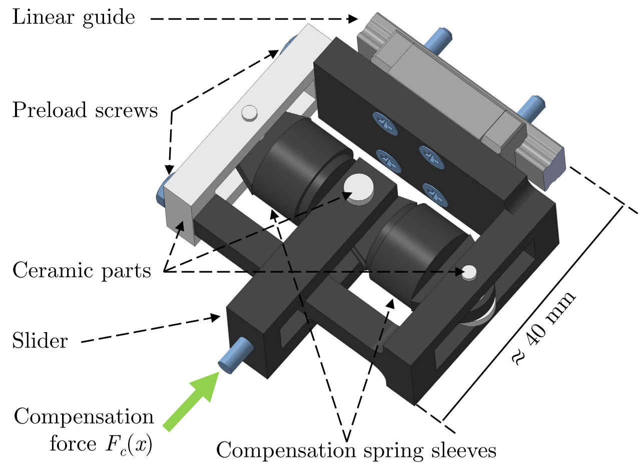

Fig. 6. CAD realization of the OSSC prototype.

This condition is particularly interesting for our application, because it minimizes the magnitude of F_n across the domain $x \in [-s, s]$. Therefore, (9) is an optimality condition for our target.

III. Design and Integration

The conceptual design of a prototype based on traditional hinges was carried out to preliminarily evaluate the applicability of the OSSC concept to the DTT ECRH launcher.

A. Mechanical Performance

Compactness is the main design driver for all components of the DTT ECRH launcher. Therefore, the OSSC prototype features the minimum number of compensation springs $n = 2$ and a lateral size $a = 20$ mm, compatible with the available space in the launcher assembly. Equations (5) and (9) were used as constraints to uniquely define the remaining OSSC parameters: condition $\beta = \beta_1$ was imposed numerically and the peak elastic resistance was reduced to 20% of its original value ($|F_n(s)| = 3.4$ N instead of $|F_e(s)| = 17$ N). Stronger compensation was avoided as it relates to compensation springs with greater free length b_0 and precompression ΔL_c, but lower

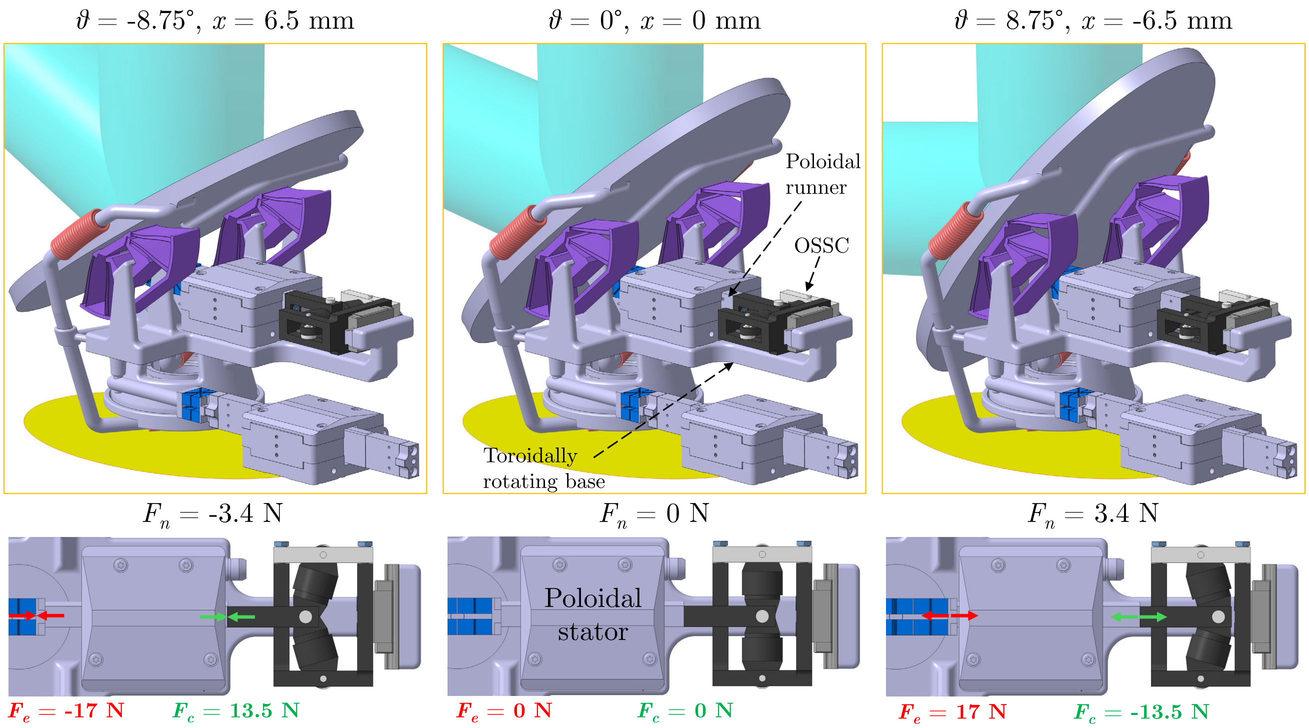

Fig. 7. Integration of the OSSC in the launcher assembly. Left and right views show end-of-stroke positions, while nominal position is shown in the center.

stiffness k_c, resulting in a difficult spring selection tradeoff. All the parameters of the OSSC can then be determined

$$\begin{aligned} k_c &= 19.7 \text{ N/mm} & k_0 &= 41.9 \text{ N/mm} \\ b_0 &= 22.15 \text{ mm} & P &= 42.2 \text{ N} \\ \Delta L_c &= 2.15 \text{ mm} & \beta &= 1.0384. \end{aligned} \tag{10}$$

Fig. 5 shows the resulting net elastic force curve. Compatible compression springs are available in many online catalogs, confirming the feasibility of the solution. For example, an AISI 302L helical spring with 9.17 mm helix diameter, 1.50 mm wire diameter, 12.70 mm free length, and 5.84 turns, would fit all requirements with a stiffness of 19.94 N/mm. A CAD realization of the resulting OSSC prototype is shown in Fig. 6.

In summary, the OSSC changes the force balance and margin against the 50 N adherence limit as follows:

Peak loads	EM	Elastic	Total	Margin
Without OSSC	30.6	17.0	47.6	2.4 N
With OSSC	30.6	3.4	35.0	15.0 N.

B. Integration in the Launcher Assembly

Fig. 7 shows how the OSSC prototype is integrated in the launcher assembly, specifically in the poloidal mechanism. The target is to add the compensating force contribution $F_c(x)$ to the elastic resistance $F_e(x) = -kx$ offered by the D-LITF, bellows and cartwheels against the actuator. Therefore, the compensator is fixed on the toroidally rotating base that also supports the poloidal stator (the fixed part of the actuator), and its slider is directly connected to the actuator runner. In order to avoid internal bending moments between OSSC and actuator, the OSSC is mounted behind the actuator, in such a way that the axis of application of F_c is coincident with the runner axis. The OSSC is connected to the base through a transverse linear guide. With direct clamping or welding, internal transverse forces due to mounting tolerances or spring-stiffness mismatch would be transmitted to the base and, more critically, to the actuator. The linear guide breaks transverse force transmission between base, OSSC, and actuator, limiting actuator transverse loads to residual guide friction. The latter can be reduced by choosing a full-ceramic guide or by replacing it with a compliant transverse slider.

C. Compatibility With Tokamak Environment

Despite the preliminary nature of the design, potential tokamak-environment effects on OSSC functionality should already be considered. The main compatibility concerns are related to EM transients, vacuum tribology, and the long-term stability of spring stiffness and preload under thermal and neutron loads. Specific constructive choices were made to limit detrimental effects related to the harsh working environment.

Ferromagnetic materials must be avoided to prevent the static magnetic field of the tokamak from producing forces on the OSSC. In particular, nonmagnetic springs like the one proposed in Section III-A must be selected. Even if this precaution is taken, it is not sufficient to prevent EM transients from inducing eddy currents and the related forces in conductive components. For this reason, large eddy current loops must be broken by including dielectric (e.g., Alumina) parts in the OSSC assembly. As shown in Fig. 6, this was implemented in the proposed design by including a ceramic side in the OSSC external frame, and ceramic pins and bushings to break the electrical contacts between the frame and the springs, which also electrically disconnects the OSSC from the actuator. Electrical insulation between the OSSC and the poloidal base can be ensured by choosing a full-ceramic linear guide or a ceramic insert between the guide and the base. The ceramic side of the frame is screwed to the metallic part to impose spring preload. If insulated as proposed, the OSSC should not experience significant EM loading under disruptions, as the large eddy current loop along the external frame is avoided, and all other loops develop in the vertical plane, which cuts a much lower magnetic flux relative to a horizontal loop. Moreover, as mentioned in Section I-B, position control is not needed during disruptions, leaving structural integrity as the only requirement, which can reasonably be ensured by the present design. Spring preloading would not suffer EM effects, while it could be affected by thermodynamic factors, which are discussed below.

The tokamak vacuum environment also makes sliding contacts potentially critical because of friction and wear. This is mitigated by avoiding metal-to-metal sliding at the spring interfaces through ceramic pins and bushings.

As far as nuclear effects are concerned, the DTT end-of-life neutron fluence in launcher region is only $2 \cdot 10^{-4}$ dpa, with negligible nuclear heating. Therefore, irradiation-induced variations of spring stiffness are expected to be limited for the present application. On the contrary, stray-radiation-induced (SRI) heating could increase components temperature above material limits and change spring preload. Two levels of protection against SRI heating will be implemented (not represented in current CAD model): the toroidally rotating base, which is connected to the mirror cooling circuit through metal bellows, will incorporate internal channels and an enveloping structure for radiative cooling of both the actuator and the OSSC. Moreover, a separate stray-radiation shield surrounding the whole steering mechanism will be designed, in order to minimize stray radiation penetration. This is needed not only to protect the OSSC and the actuators, but also the thin flexible leaves of the compliant hinges and supports. At this stage, these measures identify a feasible compatibility strategy; dedicated integrated thermo-EM verification will be part of future work.

IV. Conclusion

Among the challenges associated with the DTT ECRH launcher, one of the most critical is the limited actuation force of the piezoelectric walking drives. EM and elastic resistances are the main threats to feasibility, the former heavily depending on steering mirror design and the latter arising from the compliant elements of the transmission. This article proposed *static balancing* as a way to reduce elastic resistance. An OSSC was presented, a simple analytical model and an optimal tuning condition were derived, and a prototype integrated in the launcher assembly was conceptually designed. For the DTT launcher case, the proposed OSSC reduces the maximum elastic load transmitted to the poloidal actuator from 17 to 3.4 N, increasing the available force margin against EM disturbances while remaining compatible, at conceptual-design level, with tokamak vacuum, EM, and radiation constraints.

Acknowledgment

This work is carried out in the frame of the DTT activity, in the context of the Eni-CNR JRA. The authors are very grateful to all the colleagues involved in the DTT project for their precious contributions.

References

[1] F. Romanelli et al., "Divertor tokamak test facility project: Status of design and implementation," *Nucl. Fusion*, vol. 64, no. 11, Nov. 2024, Art. no. 112015. [Online]. Available: https://iopscience.iop.org/article/10.1088/1741-4326/ad5740

[2] G. Granucci et al., "Roles of ECH system in DTT plasma operations," *Nucl. Fusion*, vol. 64, no. 12, Dec. 2024, Art. no. 126036. [Online]. Available: https://iopscience.iop.org/article/10.1088/1741-4326/ad7742

[3] F. Fanale et al., "Status of DTT ECH transmission lines and antennae," *IEEE Trans. Plasma Sci.*, vol. 52, no. 9, pp. 3778–3784, Sep. 2024. [Online]. Available: https://ieeexplore.ieee.org/document/10498106

[4] F. Fanale et al., "Progress on the conceptual design of the antennas for the DTT ECRH system," *Fusion Eng. Design*, vol. 192, Jul. 2023, Art. no. 113797. [Online]. Available: https://www.sciencedirect.com/science/article/abs/pii/S0920379623003794

[5] R. Villari et al., "Nuclear design of divertor tokamak test (DTT) facility," *Fusion Eng. Design*, vol. 155, Jun. 2020, Art. no. 111551. [Online]. Available: https://www.sciencedirect.com/science/article/abs/pii/S0920379620300995

[6] D. Busi, F. Braghin, A. Bruschi, S. Garavaglia, G. Granucci, and A. Romano, "In-vessel piezoelectric actuation system for DTT ECRH launchers: Conceptual design," *Fusion Eng. Design*, vol. 180, Jul. 2022, Art. no. 113196. [Online]. Available: https://www.sciencedirect.com/science/article/abs/pii/S0920379622001922

[7] M. Joung et al., "Design of ECH launcher for KSTAR advanced tokamak operation," *Fusion Eng. Design*, vol. 151, Feb. 2020, Art. no. 111395. [Online]. Available: https://www.sciencedirect.com/science/article/abs/pii/S0920379619308919

[8] L. Delpech et al., "A new 3MW ECRH system at 105 GHz for WEST," *Fusion Eng. Design*, vol. 186, Jan. 2023, Art. no. 113360. [Online]. Available: https://www.sciencedirect.com/science/article/abs/pii/S0920379622003507

[9] V. Erckmann et al., "Electron cyclotron heating for W7-X: Physics and technology," *Fusion Sci. Technol.*, vol. 52, no. 2, pp. 291–312, Aug. 2007. [Online]. Available: https://www.tandfonline.com/doi/abs/10.13182/FST07-A1508

[10] S. Krebs, "Modeling of a clamping-based piezo actuator in triangular configuration," in *Proc. IEEE 17th Int. Conf. Adv. Motion Control (AMC)*, Feb. 2022, pp. 150–156. [Online]. Available: https://ieeexplore.ieee.org/document/9729314

[11] D. Busi et al., "Study of magnetic effects on DTT ECRH front-steering mirror," *Fusion Eng. Design*, vol. 191, Jun. 2023, Art. no. 113550. [Online]. Available: https://www.sciencedirect.com/science/article/pii/S0920379623001345

[12] A. Pagliaro et al., "Variable-depth complementary spiral cooling channel design for the steerable ECRH mirrors of DTT," *Fusion Eng. Design*, vol. 219, Oct. 2025, Art. no. 115276. [Online]. Available: https://www.sciencedirect.com/science/article/pii/S0920379625004727

[13] A. Pagliaro et al., "Fluid-dynamic and thermo-mechanical analyses of the metallic steering mirror for the ECRH system of DTT," *Fusion Eng. Design*, vol. 222, Jan. 2026, Art. no. 115508. [Online]. Available: https://www.sciencedirect.com/science/article/pii/S0920379625007045

[14] A. M. Sánchez, R. Chavan, T. Goodman, P. S. Silva, and M. Vagnoni, "Electromagnetic and mechanical analyses of the ITER electron cyclotron upper launcher steering M4 mirrors for the vertical displacement event," *Fusion Eng. Design*, vol. 159, Oct. 2020, Art. no. 111941. [Online]. Available: https://www.sciencedirect.com/science/article/abs/pii/S0920379620304890

[15] R. Pearce and L. Worth, "ITER vacuum handbook," ITER Org., St. Paul-lez-Durance, France, Tech. Rep. ITR-19-004, 2019. [Online]. Available: https://www.iter.org/sites/default/files/media/2024-04/iter_vacuum_handbook.pdf

[16] X. Pei, J. Yu, G. Zong, S. Bi, and Y. Hu, "A novel family of leaf-type compliant joints: Combination of two isosceles-trapezoidal flexural pivots," *J. Mech. Robot.*, vol. 1, no. 2, May 2009, Art. no. 021005. [Online]. Available: https://asmedigitalcollection.asme.org/mechanismsrobotics/article-abstract/1/2/021005/478073/A-Novel-Family-of-Leaf-Type-Compliant-Joints

[17] D. Busi, "A compact steering launcher for the electron cyclotron heating system of DTT," Ph.D. dissertation, Dept. Mech. Eng., Politecnico di Milan, Milan, Italy, 2025. [Online]. Available: https://www.politesi.polimi.it/handle/10589/236713

[18] Z. Ma, R. Zhou, and Q. Yang, "Recent advances in quasi-zero stiffness vibration isolation systems: An overview and future possibilities," *Machines*, vol. 10, no. 9, p. 813, Sep. 2022. [Online]. Available: https://www.mdpi.com/2075-1702/10/9/813

Open Access funding provided by 'Politecnico di Milano' within the CRUI CARE Agreement